Holocene dynamics of the Southern Hemisphere westerly winds and links to CO_2 outgassing

Krystyna M. Saunders*[1,2], Stephen J. Roberts[3], Bianca Perren[3], Christoph Butz[1], Louise Sime[3], Sarah Davies[4], Wim Van Nieuwenhuyze[5], Martin Grosjean[1], Dominic A. Hodgson[3,6]

[1]Institute of Geography and Oeschger Centre for Climate Change Research, University of Bern, Bern, Switzerland; [2]Australian Nuclear Science and Technology Organisation, Sydney, Australia; [3]British Antarctic Survey, Cambridge, UK; [4]Department of Geography and Earth Sciences, Aberystwyth University, Aberystwyth, UK; [5]Department of Biology, University of Ghent, Belgium; [6]Department of Geography, University of Durham, UK

*Corresponding author. KS. krystyna.saunders@ansto.gov.au

The Southern Hemisphere westerly winds (SHW) play a significant role in regulating the capacity of the Southern Ocean carbon sink. They modulate upwelling of carbon-rich deep water and, with sea ice, determine the ocean surface area available for air-sea gas exchange. Some models suggest the current strengthening and poleward shift of the SHW will weaken the carbon sink. If correct, centennial- to millennial-scale reconstructions of SHW intensity should be linked with past changes in atmospheric CO_2, temperature, and sea ice. Here, we present a 12,300-year reconstruction of wind strength based on three independent proxies that track inputs of sea salt aerosols and minerogenic particles accumulating in lake

sediments on sub-Antarctic Macquarie Island. Between c. 12.1–11.2 ka BP and since c. 7 ka BP, wind intensities were above their long-term mean, and corresponded with increasing atmospheric CO_2. Conversely, from c. 11.2–7.2 ka BP, wind intensities were below their long-term mean and corresponded with decreasing atmospheric CO_2. These observations are consistent with model inferences of enhanced SHW contributing to the long-term outgassing of CO_2 from the Southern Ocean.

The Southern Ocean currently accounts for 43 ± 3% of the global oceanic anthropogenic CO_2 uptake [1] mitigating (perhaps temporarily) the climatic effects of enhanced greenhouse gases in the atmosphere. The capacity of the Southern Ocean to absorb CO_2 at the surface is determined by the balance between processes sequestering carbon (e.g., diffusion and the biological carbon pump) versus processes releasing old carbon from the deep ocean to the atmosphere (e.g., upwelling and outgassing) [2,3]. Attempts to model these processes have yielded conflicting results. One model based on instrumental data collected between 1981 and 2004 suggested that the Southern Ocean carbon sink has weakened [4]. Conversely, analyses of the same data extended to 2011 suggest a reinvigoration of the carbon sink since 2002 [5]. This latter trend is also seen in measurements of the difference between the partial pressure of CO_2 in ocean surface water and the overlying atmosphere (ΔpCO_2) of the Southern Ocean in Drake Passage [6]. Spatial extrapolation of the relatively few pCO_2 measurements from the Southern Ocean as a whole suggests a trend towards a weakening sink in the 1990s, but a strengthening one in the 2000s [7].

45 One of the main drivers of the Southern Ocean CO_2 sink are the Southern Hemisphere westerly
46 winds (SHW), which are strongest from 50-55°S over the Southern Ocean [8] (Fig. 1a). Changes in
47 the SHW are mainly determined by atmospheric temperature gradients, sea surface
48 temperature and regional sea ice [9]. In turn they influence ocean circulation [10,11], regulate sea
49 ice extent [12] and control the upwelling of dissolved inorganic carbon-rich deep water to
50 Antarctic surface waters [2]. All are processes that modulate the net uptake of CO_2 by the ocean
51 from the atmosphere [13]. Studies that propose a weakening of the Southern Ocean CO_2 sink
52 attribute it to the recent strengthening and poleward shift of the SHW resulting from changes
53 in surface temperature gradients due to human activities, including ozone depletion [4]. This has
54 brought carbon-rich waters to the surface ocean and reduced ΔpCO_2 [1].
55
56 Despite the potential importance of the SHW in modulating net uptake of CO_2 by the Southern
57 Ocean, recent extrapolations of the future behaviour of the CO_2 sink are solely based on short-
58 term instrumental records and low spatial and temporal measurements of ΔpCO_2 [4,5]. If current
59 theories regarding a potential weakening of the CO_2 sink are correct, past reconstructions of
60 changes in the intensity of the SHW over the Southern Ocean should show clear links between
61 atmospheric CO_2, temperature and sea ice over longer (centennial-millennial) time scales.
62
63 To date, palaeoclimatic reconstructions of the SHW derive mostly from southernmost South
64 America, the only continental landmass intersecting the mid to northern core of the SHW.
65 However, they 'do not provide a consistent picture of the SHW during the Holocene' [(14, p.14)].
66 This can be partly attributed to a reliance on proxies of past changes in effective precipitation

and/or temperature to infer changes in wind strength. Examples include sub-fossil pollen assemblages in peat and lake sediment cores (e.g., [15,16]), geochemical proxies of the precipitation-evaporation balance (e.g., [17]), and rainfall changes influencing runoff into fjord [18] and ocean [19] sediments. The application of proxies that measure windblown transport (e.g., exotic pollen [20,21], dust [22]) are rare, and their relationship to wind strength not always straightforward [14].

Avoiding continental landmasses with complex orographic effects, and applying multi-proxy (and independent) methods to track past changes in wind intensity circumvents these issues. The latter tests whether different wind proxies record congruent patterns in the direction and relative magnitude of change, providing a validation that the proxies are responding to the external forcing of the SHW rather than local or internal dynamics at the study site.

We carried out a detailed reconstruction of Holocene changes in SHW intensity at sub-Antarctic Macquarie Island. The first aim was to reconstruct changes in the dynamics and relative strength of the SHW over the core jets of the Antarctic Circumpolar Current; the region most relevant to Southern Ocean air-sea gas exchange [23]. The second was to test which of the competing models of a weakening [4] or reinvigoration [5] of the carbon sink in recent decades is supported by the long-term palaeo-record. We did not consider changes in the position of the SHW core belt (50-55°S) in detail. More well-dated, multi proxy records are needed from broader latitudinal and longitudinal ranges to reliably separate changes in intensity from changes in latitudinal position.

Sub-Antarctic Macquarie Island

Macquarie Island is a small, 130 km^2, sub-Antarctic island located a few hundred kilometres north of the Polar Front (54°S, 158°E; Fig. 1 and Supplementary Note 1). The sub-Antarctic islands are the only landmasses, other than southernmost South America, that lie in the core of the SHWs. Macquarie Island experiences mean annual wind speeds of ~35 km hr^{-1}, a mean daily wind run of 751 km, gusts of up to 185 km hr^{-1} [24] and its climate is representative of the core belt of the SHW (Fig. 1 c, d). Wind almost exclusively comes from the west-northwest (Supplementary Figs. 2 and 3). This results in strong west to east gradients in sea-spray [25] and minerogenic wind-blown aerosols being deposited across the island. These aerosols accumulate over time in lake and peat sediments, preserving a record of relative changes in SHW intensity, with periods of more (or less) sea spray or deposited minerogenic material reflecting phases of stronger (or weaker) winds. We applied a combination of three methods to reconstruct past changes in SHW intensity using a sedimentary sequence from Emerald Lake, a small lake perched on the western edge of the Macquarie Island plateau, and directly exposed to westerly air flow (Supplementary Note 2). The sediment sequence was radiometrically dated with 44 ^{14}C and 11 ^{210}Pb dates (Supplementary Note 3). Freshwater diatom-based inference models provided a measure of past sea spray aerosol inputs through their effect on the conductivity and diatom species assemblages in lakes [25]. These were compared with two independent measures of minerogenic aerosol inputs based on micro X-ray fluorescence (μ-XRF) core scanning and hyperspectral imaging. These proxies, and the sedimentology of the core, are described in Supplementary Notes 4, 5.

111

112 **Holocene dynamics of the SHW**

113 The three proxies used in the present study show similar patterns in wind strength over
114 Macquarie Island over the last c. 12.3 ka BP (Fig. 2, Supplementary Note 5). The strongest
115 correlation is between the two methods measuring minerogenic inputs ($r=0.85$, $p<0.0001$,
116 Supplementary Table 4). These are also significantly correlated with the independent diatom-
117 inferred conductivity / sea spray proxy ($r=0.56$ and $r=0.65$, $p<0.0001$). The slightly weaker
118 correlations with the diatom-inferred conductivity / sea spray proxy can be attributed to lake
119 water nutrients and pH which explain smaller yet independent portions of the variance in the
120 diatom data [25]. The correlations between the minerogenic wind proxies and diatom-inferred
121 conductivity excludes changes in dust supply from source regions as a major factor modifying
122 the reconstructions. The period from 7.5–7.2 ka BP shows a negative correlation between the
123 minerogenic proxies and diatom-inferred conductivity. Based on the presence of sub-aerial
124 diatoms, this was attributed to a brief period of low water levels (see Supplementary Note 4).

125

126 In general, the proxies show high relative wind intensity (defined here as periods when at least
127 two of the three wind proxies have values greater than the 95% upper bound of their mean,
128 Supplementary Table 6) between 12.1–11.2, 9.2–8.5, 7.9–7.7, 7.0–5.6, 5.3–0.2 and 0.1–0 ka BP.
129 Low relative wind intensities were recorded from 11.2–9.2, 8.4–7.9, 7.7–7.0 and 0.2–0.1 ka BP.
130 The key features are high relative winds spanning the end of the Last Glacial-Interglacial
131 Transition (LGIT) to the early Holocene (12.1–11.2 ka BP), low relative winds during the early
132 Holocene Thermal Maximum (11.2–9.2 ka BP), increased winds and higher amplitude changes

between 9.2–5.3 ka BP, and a period of sustained relatively intense winds from 5.3 to 0.2 ka BP (although the resolution of the record is lower during this period) (Fig. 2). After 0.2 ka BP the wind intensity drops and then increases in the most recent decades.

SHW dynamics, atmospheric CO_2, sea ice and temperature

Significant correlations between the three independent wind proxies support the hypothesis that, together, they provide a reliable record of changes in the dynamics of the SHW in their core belt, and more specifically at Macquarie Island. Therefore, to address our wider objective of evaluating the role of the SHW as a driver of natural CO_2 variations, we compared past changes in the SHW at Macquarie Island with other hemispheric changes in the ocean and atmosphere. These include far-field proxy records in the EPICA Dome C ice core of sea ice (sea salt Na+ aerosol flux)[26], temperature and CO_2[2], and marine core microfossil-based measurements of winter sea ice concentration (WSI %) in selected (and not necessarily representative) marine cores from the South Atlantic (PS2090[27]) and South Pacific sector near Macquarie Island (E27-23[28], Fig. 3).

12.1–11.2 ka BP: The end of the LGIT and early Holocene are characterised by intense SHW. Many records at similar latitudes in southernmost South America (Supplementary Fig. 15c-e), and elsewhere in the Southern Hemisphere (Supplementary Note 7) agree. This period of intense SHW is accompanied by marked increases in atmospheric CO_2 and temperature (Fig 3e, f), and declines in sea ice (Fig. 3c, d). There are both proxy and model-based studies that support the magnitude and direction of these changes across the LGIT [10,29,30]. Specifically, the

155 persistent winds identified here are consistent with enhanced Southern Ocean upwelling [10]
156 accounting for at least part of the deglacial rise in atmospheric CO_2, and accompanied by
157 increases in atmospheric [30] and sea surface temperatures [29]. Temporal patterns in our records
158 are also consistent with the retreat of sea ice having a positive feedback on the ocean surface
159 area available for the outgassing of CO_2 [29] (Fig. 3).
160
161 ***11.2–9.2 ka BP:*** An early Holocene Thermal Maximum between 11.2–9.2 ka BP is clearly
162 resolved in Antarctica [31] and other records across the Southern Hemisphere, including the
163 western side of the Andes from 49–55°S [14]. This reduced the thermal gradient between the mid
164 and high latitudes and resulted in persistent low intensity winds at Macquarie Island (Fig. 3a, b).
165 This is consistent with selected records from South America [32,33], Tasmania and New Zealand [32]
166 (Supplementary Note 7), and a reduced thermal gradient in the Southern Ocean east and south
167 of New Zealand [34]. If replicated in further studies, this would suggest a widespread decrease in
168 wind intensity across the Southern Hemisphere from 41°S to 54°S (Macquarie Island, see
169 Supplementary Note 7). The sustained warm conditions and low wind intensity during this
170 period corresponded with reduced sea ice in marine [27,29] and ice core records [35], and was
171 followed by the only long-term decline in atmospheric CO_2 (c. 10.5–7.2 ka BP) since the
172 Antarctic Cold Reversal [36].
173
174 ***9.2–5.3 ka BP:*** All three wind proxies at Emerald Lake show a period of increased and higher
175 amplitude changes in wind intensity (relative to the early Holocene Thermal Maximum),
176 punctuated by relatively shorter lived (multi-centennial) periods when wind strength is

significantly lower. This corresponds to some terrestrial records of enhanced precipitation in South America (e.g., Tamar Lake [32] and Lago Cipreses [33], but not others [8]; see Supplementary Note 7). These increased winds coincide with a downturn in temperature and increases in sea ice (Fig. 3c, d). During the first part of this period the positive relationship between enhanced winds and sea ice appears similar to the beginning of the record (12.1–11.2 ka BP), but differs, at least until 7 ka BP, because the winds did not correspond with an increase in atmospheric CO_2 (Fig. 3f). We attribute this to the concurrent development of alternative carbon sinks in the terrestrial biosphere, including mineral soils, peat and permafrost carbon [37,38]. However, after 7 ka BP, increased wind strength and sea ice correspond to the onset of the steady increase in atmospheric CO_2 that characterised the middle and late Holocene.

5.3–0 ka BP: This period of relatively constant and intense winds at Macquarie Island and elevated rainfall inferred from several studies on the western side of the Andes (see Supplementary Note 7, Supplementary Fig 15) corresponds with: relatively high sea ice in the Atlantic sector (Fig. 3c); increases in the ice core ssNa after 4 ka (Fig. 3d); a sustained increase in atmospheric CO_2 (Fig. 3f). Combined, this evidence implies that persistent strong winds led to net Southern Ocean outgassing during the latter part of the Holocene. Over the last 0.2 ka BP, our record of Ti aerosol inputs into Emerald Lake show an initial decline, followed by an increase in the last c. 100 years. The latter is consistent with instrumental records from Macquarie Island, and other areas of the Southern Ocean, which have shown an intensification and southward shift in the main wind belt [5] (Supplementary Fig. 2). However, during this period,

198 all proxies are potentially compromised by erosional inputs associated with the activities of
199 introduced species [39] ('rabbit-influenced zone'; Fig. 2).
200
201 **SHW, CO_2, temperature and sea ice**
202 To develop our understanding of Southern Hemisphere climate dynamics, we now focus on the
203 centennial to millennial relationships between the SHW, atmospheric CO_2, temperature and sea
204 ice, and the extent to which they are replicated in selected Global Climate Models.
205
206 First, the Macquarie record shows significant positive relationships between SHW and sea ice
207 particularly through the late LGIT and early Holocene, and possibly during the period of
208 sustained relatively intense winds from 5.3 to 0.2 ka BP (Supplementary Table 4,
209 Supplementary Note 5). This is consistent with CMIP5 models that show significant
210 relationships between SHW jet strength and sea ice area [40]. It has been suggested that a
211 strengthened SHW jet leads to increased Ekman upwelling bringing cooler subsurface water to
212 the surface and strengthened equatorward transport, which is conducive to increased sea ice [12].
213 Alternatively, at least part of the correspondence between the SHW reconstruction and ice core
214 ssNA could be attributed to direct wind-driven transport of ssNa to the Dome C ice core site,
215 independent of changes in sea ice extent, although this has previously been questioned based
216 on chemical signatures in the ice [41]. Thus, except for the 9.2–7 ka BP period, where the
217 relationship is less clear, the Macquarie Island record suggests that, at centennial to millennial
218 timescales during the Holocene, sea ice and the intensity of the SHW were broadly in phase.
219

Second, in terms of the relationship between the SHW and atmospheric temperature and CO_2, the Macquarie Island proxy records show that windier periods (i.e., greater than the 95% upper bound of their long-term mean) correspond with periods of increasing atmospheric CO_2 (orange boxes in Fig. 3b, f) from 12.1–11.2 ka BP, and in the last 7 ka. Conversely, the period of lower than mean winds from 11.2 ka BP corresponds with decreasing atmospheric CO_2 (blue boxes in Fig. 3b, f), and a downturn in temperature (Fig. 3e), which persisted until c. 8 ka BP. This relationship is reproduced in short term CMIP5 model experiments, which consistently show a poleward shift and strengthening of the SHW jet in response to increasing greenhouse gases and stratospheric ozone [42]. These observations are consistent with enhanced wind driven upwelling of CO_2 rich deep ocean waters, accounting for at least part of the increase in atmospheric CO_2 across the LGIT and into the early Holocene [3] and the last 7ka, whilst periods of reduced wind strength enhance the Southern Ocean CO_2 sink. The larger magnitude of the increase in CO_2 during the late LGIT and early Holocene (Fig. 3) can be attributed to the higher CO_2 available for release from the glacial deep ocean [43]. In contrast, the moderate increases in CO_2 since 7 ka BP can be attributed to less CO_2 available for release from the ocean and the development of terrestrial carbon sinks [37].

SHW and the future of the Southern Ocean carbon sink

Our new records of the SHW, which are aligned with the core jets of the present-day Antarctic Circumpolar Current, suggest large changes in wind intensity over the last 12.1 ka BP. This is in marked contrast to model simulations of the SHW across the Last Glacial termination and Holocene which simulate only relatively small wind speed anomalies (± 1 m s^{-1}) [9,23,44,45]. The

correspondence between strong and persistent SHW and the rise in CO_2 during the latter part of the LGIT into the early Holocene, and from 7 ka BP suggests that the winds have contributed to the long-term outgassing of CO_2 from the ocean during these periods. This provides a longer-term perspective on the 30-year instrumental record of ΔpCO_2 and SHW strength, which has been used to evaluate short-term changes in the behaviour of the Southern Ocean carbon sink [4,5]. Specifically, the palaeo-data support the Le Quéré model [4], which suggests a wind-driven weakening of the Southern Ocean carbon sink (enhanced outgassing) prior to 2007 CE as the dominant process. It does not support the alternative Landschützer model [5], which proposes that a stabilisation of the surface waters has counteracted the wind induced upwelling and reinvigorated the carbon sink during the last decade. Therefore, over multi-decadal to millennial timescales, further increases in wind strength will lead to faster accumulation of CO_2 in the atmosphere.

Methods

A series of lake sediment cores dating back to c. 12.1 ka BP were extracted from Emerald Lake on the western edge of the Macquarie Island plateau. Perched within a small catchment, Emerald Lake is ideally situated to record changes in sea salt and mineral aerosol inputs (Supplementary Notes 2, 3). We applied three independent methods to reconstruct past changes in SHW intensity (Supplementary Note 5). First, to reconstruct past sea salt aerosol inputs, we developed a method to track past changes in lake water conductivity (a function of sea salt aerosol input) using diatom-based inference models [25,46]. These utilise the strong statistical relationship between modern diatom species assemblages and lake water

conductivity (weighted averaging partial least squares, two components; $r^2 = 0.92$, $r^2_{jack} = 0.72$, RMSEP = 230 µS cm^{-1} (Supplementary Note 5), which is applied as a transfer function to reconstruct past changes in conductivity from subfossil species assemblages preserved in lake sediments. Second, ITRAX™ micro X-ray fluorescence (µ-XRF) core scanner data were used to track inputs of minerogenic aerosols into the lake, focusing on titanium (Ti), one of the most widely used indicator elements for increased allochthonous inputs [47] from distal and proximal sources [48]. Third, cores were scanned using a Specim hyperspectral camera, which measures reflected optical properties between wavelengths from 400–1000 nm [49]. The ratio of reflectance between 850 and 900 nm (R_{850}/R_{900}) was used as an additional indicator of minerogenic inputs. Statistical analyses of the proxies were undertaken using R 2.15.2 (R Foundation for Statistical Computing), MATLAB® (Supplementary Note 3 for details) and in Sigmaplot v13, using original and 100-year interval 2nd order polynomial LOESS (Local tricube weighting and polynomial regression) smoothing. The calibration and performance of each of these methods together with details of core sedimentology and chronology are described in Supplementary Notes 3, 4 and 5. Potential influences on the proxies (e.g., lake ice cover and relative sea level) are described in Supplementary Note 6.

Data Availability

All data are archived at the Australian Antarctic Data Centre (https://data.aad.gov.au/) and Natural Environment Research Council Polar Data Centre (https://www.bas.ac.uk/data/uk-pdc/).

References

1 Mikaloff-Fletcher, S. E. CLIMATE. An increasing carbon sink? *Science* **349**, 1165, doi:10.1126/science.aad0912 (2015).

2 Hodgson , D. A. & Sime, L. C. Southern westerlies and CO_2. *Nat. Geosci.* **3**, 666-667, doi:610.1038/ngeo1970 (2010).

3 Toggweiler, J. R., Russell, J. L. & Carson, S. R. Midlatitude westerlies, atmospheric CO2, and climate change during the ice ages. *Palaeoceanography* **21** PA2005 doi:10.1029/2005PA001154 (2006).

4 Le Quéré, C. *et al.* Saturation of the Southern Ocean CO2 Sink Due to Recent Climate Change. *Science* **316**, 1735 - 1738 (2007).

5 Landschützer, P. *et al.* The reinvigoration of the Southern Ocean carbon sink. *Science* **349**, 1221-1224, doi:10.1126/science.aab2620 (2015).

6 Munro, D. R. *et al.* Recent evidence for a strengthening CO_2 sink in the Southern Ocean from carbonate system measurements in the Drake Passage (2002–2015). *Geophys. Res. Lett.* **42**, 2015GL065194, doi:10.1002/2015GL065194 (2015).

7 Ritter, R. *et al.* Observation-Based Trends of the Southern Ocean Carbon Sink. *Geophys. Res. Lett.* **44**, 12,339-312,348, doi:doi:10.1002/2017GL074837 (2017).

8 Lamy, F. *et al.* Holocene changes in the position and intensity of the Southern Westerly wind belt. *Nat. Geosci.* **3**, 695-699 (2010).

9 Sime, L. C. *et al.* Southern Hemisphere westerly wind changes during the Last Glacial Maximum: model-data comparison. *Quaternary Sci. Rev.* **64**, 104-120 (2013).

10 Anderson, R. F. *et al.* Wind-Driven Upwelling in the Southern Ocean and the Deglacial Rise in Atmospheric CO2. *Science* **323**, 1443 - 1448 (2009).

11 Lovenduski, N. S., Gruber, N. & Doney, S. C. Toward a mechanistic understanding of the decadal trends in the Southern Ocean carbon sink. *Global Biogeochem. Cy.* **22**, n/a-n/a, doi:10.1029/2007GB003139 (2008).

12 Purich, A., Cai, W., England, M. H. & Cowan, T. Evidence for link between modelled trends in Antarctic sea ice and underestimated westerly wind changes. *Nat. Commun.* **7**, 10409, doi:10.1038/ncomms10409, http://www.nature.com/articles/ncomms10409#supplementary-information (2016).

13 Wanninkhof, R. *et al.* Global ocean carbon uptake: magnitude, variability and trends. *Biogeosciences* **10**, 1983-2000, doi:10.5194/bg-10-1983-2013 (2013).

14 Kilian, R. & Lamy, F. A review of Glacial and Holocene paleoclimate records from southernmost Patagonia (49–55°S). *Quaternary Sci. Rev.* **53**, 1-23, doi:http://dx.doi.org/10.1016/j.quascirev.2012.07.017 (2012).

15 Fontana, S. L. & Bennett, K. Postglacial vegetation dynamics of western Tierra del Fuego. *Holocene* **22**, 1337-1350, doi:doi:10.1177/0959683612444144 (2012).

16 Waldmann, N. *et al.* Integrated reconstruction of Holocene millennial-scale environmental changes in Tierra del Fuego, southernmost South America. *Palaeogeogr., Palaeocl.* **399**, 294-309, doi:http://dx.doi.org/10.1016/j.palaeo.2014.01.023 (2014).

17 Moy, C. M. *et al.* Isotopic Evidence for Hydrologic Change Related to the Westerlies in SW Patagonia, Chile During the Last Millennium. *Quaternary Sci. Rev.* **27**, 1335-1349 (2008).

18 .Bertrand, S., Hughen, K., Sepúlveda, J. & Pantoja, S. in *Supplement to: Bertrand, S et al. (2014): Late Holocene covariability of the southern westerlies and sea surface temperature in Northern Chilean Patagonia. Quaternary Sci. Rev., 105, 195-208, doi:10.1016/j.quascirev.2014.09.021* (PANGAEA, 2014).

19 Lamy, F. *et al.* Antarctic Timing of Surface Water Changes off Chile and Patagonian Ice Sheet Response. *Science* **304**, 1959 - 1962 (2004).

20 Strother, S. L. *et al.* Changes in Holocene vegetation, climate and the intensity of Southern Hemisphere Westerly Winds based on a high-resolution palynological record from sub-Antarctic South Georgia. *Holocene* **25**, 263-279 (2015).

21 Turney, C. S. M. *et al.* A 250-year periodicity in Southern Hemisphere westerly winds over the last 2600 years. *Clim. Past* **12**, 189-200, doi:10.5194/cp-12-189-2016 (2016).

22 Vanneste, H. *et al.* Late-glacial elevated dust deposition linked to westerly wind shifts in southern South America. *Sci. Rep.* **5, 11670, doi:10.1038/srep11670** (2015).

23 Sime, L. C. *et al.* Sea ice led to poleward-shifted winds at the Last Glacial Maximum: the influence of state dependency on CMIP5 and PMIP3 models. *Clim. Past* **12**, 2241-2253, doi:10.5194/cp-12-2241-2016 (2016).

24 Australian-Government-Bureau-of-Meterology. *Climate statistics for Australian locations, Macquarie Island*, <http://www.bom.gov.au/climate/averages/tables/cw_300004_All.shtml> (2017).

25 Saunders, K. M., Hodgson, D. A. & McMinn, A. Quantitative relationships between benthic diatom assemblages and water chemistry in Macquarie Island lakes and their

potential to reconstruct past environmental changes. *Antarct. Sci.* **21**, 35-49, doi:10.1017/S0954102008001442 (2009).

26 Röthlisberger, R. *et al.* Dust and sea salt variability in central East Antarctica (Dome C) over the last 45 kyrs and its implications for southern high-latitude climate. *Geophys. Res. Lett* **29**, 24-21-24-24, doi:10.1029/2002GL015186 (2002).

27 Xiao, W., Esper, O. & Gersonde, R. Last Glacial - Holocene climate variability in the Atlantic sector of the Southern Ocean. *Quaternary Sci. Rev.* **135**, 115-137, doi:http://dx.doi.org/10.1016/j.quascirev.2016.01.023 (2016).

28 Ferry, A. J. *et al.* First records of winter sea ice concentration in the southwest Pacific sector of the Southern Ocean. *Paleoceanography* **30**, 1525-1539, doi:10.1002/2014PA002764 (2015).

29 Bianchi, C. & Gersonde, R. Climate evolution at the last deglaciation: the role of the Southern Ocean. *Earth Planet. Sc. Letters* **228**, 407-424, doi:http://dx.doi.org/10.1016/j.epsl.2004.10.003 (2004).

30 Jouzel, J. *et al.* Orbital and Millennial Antarctic Climate Variability over the Past 800,000 Years. *Science* **317**, 793-796, doi:10.1126/science.1141038 (2007).

31 Masson, V. *et al.* Holocene climate variability in Antarctica based on 11 ice-core isotope records. *Quaternary Res.* **54**, 348-358 (2000).

32 Fletcher, M.-S. & Moreno, P. I. Zonally symmetric changes in the strength and position of the Southern Westerlies drove atmospheric CO_2 variations over the past 14 k.y. *Geology* **DOI: 10.1130/G31807.1** (2011).

33 Moreno, P. I. *et al.* Onset and Evolution of Southern Annular Mode-Like Changes at Centennial Timescale. *Sci. Rep.* **8**, 3458, doi:10.1038/s41598-018-21836-6 (2018).

34 Prebble, J.G.. *et al.* Evidence for a Holocene Climatic Optimum in the southwest Pacific: A multiproxy study. *Paleoceanography* **32**, 763-779, doi:doi:10.1002/2016PA003065 (2017).

35 Röthlisberger, R. in *Data Contribution Series #2005-046* (ed IGBP PAGES/World Data Center for Paleoclimatology) (NOAA/NGDC Paleoclimatology Program, Boulder CO, USA, 2005).

36 Monnin, E. *et al.* Atmospheric CO_2 Concentrations over the Last Glacial Termination. *Science* **291**, 112-114, doi:10.1126/science.291.5501.112 (2001).

37 Brovkin, V. *et al.* Comparative carbon cycle dynamics of the present and last interglacial. *Quaternary Sci. Rev.* **137**, 15-32, doi:https://doi.org/10.1016/j.quascirev.2016.01.028 (2016).

38 Stocker, B. D., Yu, Z., Massa, C. & Joos, F. Holocene peatland and ice-core data constraints on the timing and magnitude of CO_2 emissions from past land use. *P. Natl. A. Sci.* **114**, 1492-1497, doi:10.1073/pnas.1613889114 (2017).

39 Saunders, K. M. *et al.* Ecosystem impacts of feral rabbits on World Heritage sub-Antarctic Macquarie Island: A palaeoecological perspective. *Anthropocene* **3**, 1-8 (2013).

40 Bracegirdle, T. J., Hyder, P. & Holmes, C. R. CMIP5 Diversity in Southern Westerly Jet Projections Related to Historical Sea Ice Area: Strong Link to Strengthening and Weak Link to Shift. *J.. Climate* **31**, 195-211, doi:10.1175/jcli-d-17-0320.1 (2018).

41 Wolff, E. W. *et al.* Southern Ocean sea-ice extent, productivity and iron flux over the past eight glacial cycles. *Nature* **440**, 491-496 (2006).

42 Bracegirdle, T. J. *et al.* Assessment of surface winds over the Atlantic, Indian, and Pacific Ocean sectors of the Southern Ocean in CMIP5 models: historical bias, forcing response, and state dependence. *J. Geophys. Res.-Atmos.* **118**, 547-562, doi:10.1002/jgrd.50153 (2013).

43 Peter, K., Hubertus, F., Guy, M. & E., Z. R. Quantitative interpretation of atmospheric carbon records over the last glacial termination. *Global Biogeochem. Cy.* **19**, doi:doi:10.1029/2004GB002345 (2005).

44 Chavaillaz, Y., Codron, F. & Kageyama, M. Southern westerlies in LGM and future (RCP4.5) climates. *Clim. Past* **9**, 517-524, doi:10.5194/cp-9-517-2013 (2013).

45 Rojas, M. Sensitivity of Southern Hemisphere circulation to LGM and 4 × CO2 climates. *Geophys. Res. Lett.* **40**, 965-970, doi:10.1002/grl.50195 (2013).

46 Van Nieuwenhuyze, W. *Reconstruction of Holocene paleoenvironmental changes in the sub-Antarctic region* PhD thesis, University of Ghent, (2015).

47 Davies, S. J., Lamb, H. F. & Roberts, S. J. in *Micro-XRF Studies of Sediment Cores, Developments in Palaeoenvironmental Research series,* (eds Croudace IW & Rothwell RG) (Springer, 2015).

48 Heimburger, A., Losno, R., Triquet, S. & Nguyen, E. B. Atmospheric deposition fluxes of 26 elements over the Southern Indian Ocean: Time series on Kerguelen and Crozet Islands. *Global Biogeoch. Cy.* **27**, 440-449, doi:10.1002/gbc.20043 (2013).

49 Butz, C. *et al.* Hyperspectral imaging spectroscopy: A promising method for the biogeochemical analysis of lake sediments. *J. Appl. Remote Sens.* **9**, doi:10.1117/1111.JRS.1119.096031 (2015).

Acknowledgements: This research was funded by NERC-Standard Grant NE/K004514/1 (DH, SR, LS), Swiss National Science Foundation Ambizione Postdoctoral Research Fellowship PZ00P2_136835/1 (KS), Swiss National Science Foundation Grant 200021_172586 (MG), and Australian Antarctic Science grants 3117 and 4156 (KS). KS was also supported by PhD funding as part of grant 2663 to Professor Andrew McMinn, an Australian Postgraduate Award (2004–2008), and an Australian Institute of Nuclear Science and Engineering Postgraduate Research Award. The Australian Antarctic Division and the Parks and Wildlife Service Tasmania provided logistical support and access to the Macquarie Island World Heritage Area. Field support was provided by Anthony O'Hern, Andrew Wakefield, Chris Oosthuizen, Ben Arthur, Josie van Dorst, James Pitcher, Scottie Williams, Tyrone Blyth, Parks and Wildlife Service Rangers and volunteers. Special thanks to Hua Lu of the British Antarctic Survey for providing and adapting MATLAB® scripts for SMKT analyses, Alex Whittle for processing the wind data and underlying geotifs in Figure 1a, b, Daniela Fischer, Stéphanie Arcusa and Neil Tunstall for technical support.

Author contributions

DH, KS and SR contributed equally to this work. Fieldwork was carried out by KS, DH, SR, WVN. Analytical work was performed by SR (micro-XRF, sedimentology, chronology, statistical analyses) and SD (micro-XRF), KS and BP (D-I conductivity analyses, chronology, sedimentology),

WVN (fieldwork, diatom analysis), KS, CB and MG (hyperspectral imaging) and LS (modelling). DH, KS, SR and BP wrote the manuscript and supplementary information with input from all authors.

Competing Interests statement: The authors declare no competing financial interests

Figure captions

Figure 1. Southern Hemisphere westerly winds and wind anomalies in relation to the location of Macquarie Island (white circle) a. Location of Macquarie Island in the Southern Ocean within the core of the Southern Hemisphere Westerly wind (SHW) belt. White square = EPICA Dome C ice core (EDC). Grey triangle = marine core PS2090, white triangle = marine core E27-23; SHW = Southern Hemisphere Westerlies, PF = Polar Front, SACCF = Southern Antarctic Circumpolar Current Front. **b.** Location of Macquarie Island and Emerald Lake (pansharpened LANDSAT8 satellite image, bands 4,3,2). **c.** Annual mean and **d.** Decadal wind speed anomalies associated with the top 20% of highest wind speed events at Macquarie Island (see Supplementary Notes 1 and 2 for details).

Figure 2. Changes in relative strength of the Southern Hemisphere westerly winds based on proxies in a sediment core from Emerald Lake. a. Diatom-inferred (D-I) conductivity. **b.** Titanium (Ti) micro-XRF analysis. **c.** Micro-XRF Principal Components Analysis Axis 1. **d.** Hyperspectral ratios (R_{850}/R_{900}). Red lines = 100-year interval 2nd order LOESS-smoothing.

Periods of increased wind strength defined as > than the 95% upper bound of the mean (blue horizontal lines; see Supplementary Note 5 and Supplementary Table 6). Green shading indicates when proxies compromised by erosional inputs from non-indigenous species [42]. LGIT = Last Glacial–Interglacial Transition, EH = early Holocene, MH = mid Holocene, LH = late Holocene. Horizontal bar = formal EH. Lithology described in Supplementary Table 3 and Note 4.

Figure 3. Comparison of Macquarie Island wind proxies with sea ice, temperature and CO_2 a. Diatom-inferred (D-I) conductivity **b.** Titanium (Ti) micro-XRF data. **c.** Southern Ocean winter sea ice concentration (WSIC) from marine cores PS2090 [29] and E27-23 [30]. **d.** EPICA Dome C sea salt Na^+ aerosol flux (representing new sea ice surfaces) [38]. **e.** EPICA Dome C temperature anomaly [32]. **f.** EPICA Dome C CO_2 [39]. Grey dotted lines are lithological zones defined in Figure 2. Orange highlights periods when above-mean winds correspond to increasing CO_2, blue when below-mean winds correspond to decreasing CO_2. LGIT = Last Glacial–Interglacial Transition, EH = early Holocene, MH = mid Holocene, LH = late Holocene. Horizontal bar = formal EH.

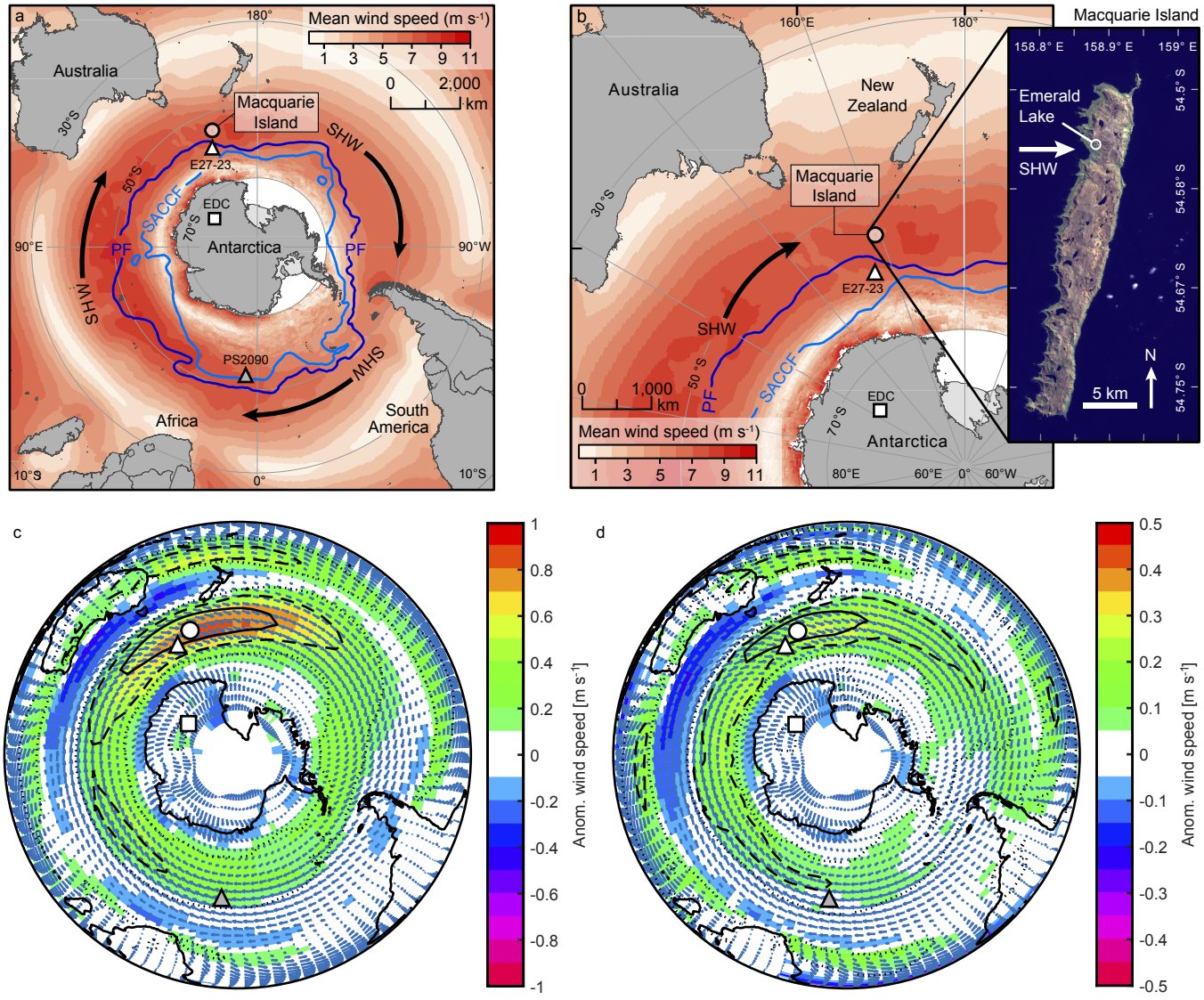
a
Mean wind speed (m s-1)
1 3 5 7 9 11
0 2,000 km
Australia
Macquarie Island
E27-23
EDC
Antarctica
PS2090
Africa
South America
SHW
MHS
SACCF
PF
50°S
70°S
30°S
10°S
90°E
90°W
180°
0°
b
Macquarie Island
160°E
180°
New Zealand
Australia
Macquarie Island
E27-23
EDC
Antarctica
SHW
SACCF
PF
50°S
70°S
30°S
0 1,000 km
Mean wind speed (m s-1)
1 3 5 7 9 11
80°E
60°E
0°
60°W
158.8° E
158.9° E
159° E
54.5° S
54.58° S
54.67° S
54.75° S
Emerald Lake
SHW
N
5 km
c
d
Anom. wind speed [m s-1]
1
0.8
0.6
0.4
0.2
0
-0.2
-0.4
-0.6
-0.8
-1
0.5
0.4
0.3
0.2
0.1
0
-0.1
-0.2
-0.3
-0.4
-0.5

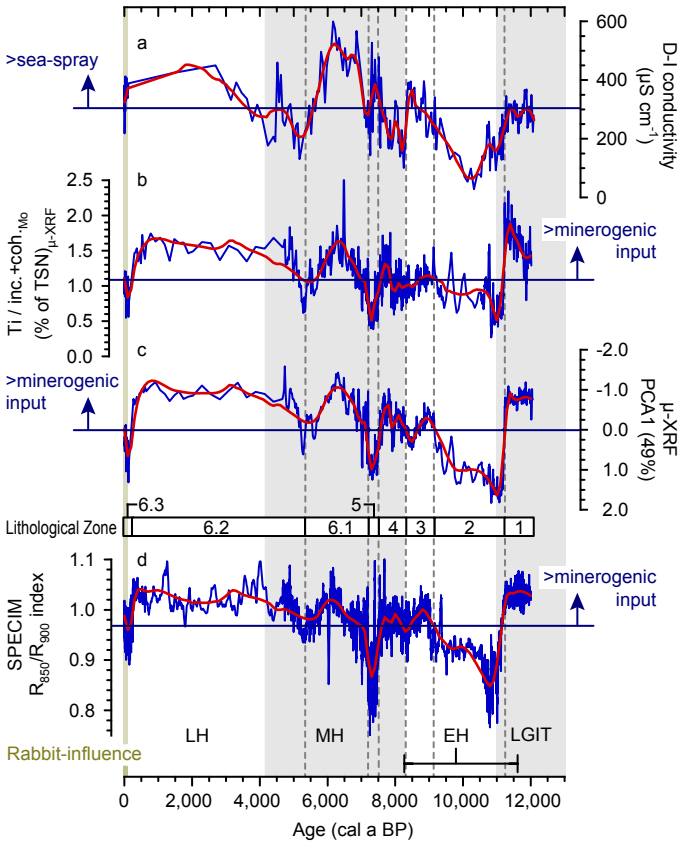
a
>sea-spray
600
400
200
0
D-I conductivity (µS cm-1)
b
2.5
2.0
1.5
1.0
0.5
0.0
Ti / inc.+coh-Mo (% of TSN)µ-XRF
>minerogenic input
c
>minerogenic input
-2.0
-1.0
0.0
1.0
2.0
µ-XRF PCA1 (49%)
6.3
5
Lithological Zone
6.2
6.1
4
3
2
1
d
1.1
1.0
0.9
0.8
SPECIM R850/R900 index
>minerogenic input
LH
MH
EH
LGIT
Rabbit-influence
0
2,000
4,000
6,000
8,000
10,000
12,000
Age (cal a BP)

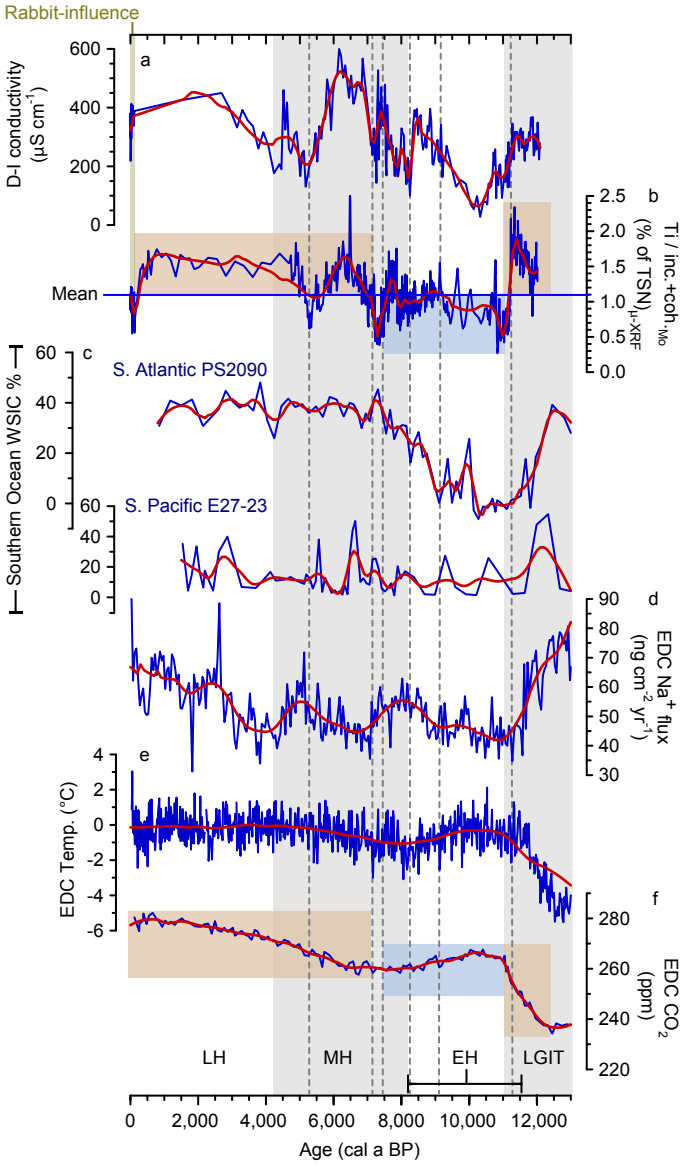
Rabbit-influence
a
D-I conductivity (µS cm⁻¹)
600
400
200
0
Mean
b
Ti / inc.+coh.Mo (% of TSN)µ-XRF
2.5
2.0
1.5
1.0
0.5
0.0
c
Southern Ocean WSIC %
S. Atlantic PS2090
S. Pacific E27-23
60
40
20
0
d
EDC Na+ flux (ng cm-2 yr-1)
90
80
70
60
50
40
30
e
EDC Temp. (°C)
4
2
0
-2
-4
-6
f
EDC CO2 (ppm)
280
260
240
220
LH
MH
EH
LGIT
0
2,000
4,000
6,000
8,000
10,000
12,000
Age (cal a BP)